Available online at www.sciencedirect.com
SCIENCE DIRECT®
Journal of Catalysis 219 (2003) 259–272
JOURNAL OF CATALYSIS
www.elsevier.com/locate/jcat

Mathematical modeling of the oxygen storage capacity phenomenon studied by CO pulse transient experiments over Pd/CeO_2 catalyst

C.N. Costa,[a] S.Y. Christou,[a] G. Georgiou,[b] and A.M. Efstathiou [a,*]

[a] *Department of Chemistry, University of Cyprus, PO Box 20537, Nicosia, Cyprus*
[b] *Department of Mathematics and Statistics, University of Cyprus, PO Box 20537, Nicosia, Cyprus*

Received 4 December 2002; revised 3 March 2003; accepted 21 March 2003

Abstract

A mathematical model has been developed for the first time to study the oxygen storage capacity (OSC) phenomenon by the CO pulse injection technique over a 1 wt% Pd/CeO_2 model catalyst in the 500–700 °C range. A two-step reaction path that involves the reaction of gaseous CO with the oxygen species of PdO (pre-oxidized supported palladium particles in the 500–700 °C range) and of the back-spillover of the oxygen process from ceria to the oxygen vacant sites of surface PdO has been proven to better describe the outlet CO pulse transient response and the experimentally measured quantity of OSC (μatoms of O/g) obtained in a CSTR microreactor. With the proposed mathematical model, the transient rates of the CO oxidation reaction and of the back-spillover of the oxygen process can be calculated. In the 500–700 °C range, the transient rate of CO oxidation was always greater than that of the back-spillover of oxygen. The ratio, ρ, of the maximum CO oxidation rate to the maximum back-spillover of the oxygen rate was found to decrease with increasing reaction temperature in the 500–700 °C range. In particular, at 500 and 700 °C the value of ρ was found to be 1.6 and 1.2, respectively. The present mathematical model allows also the calculation of the intrinsic rate constant k_1 (s^{-1}) of the Eley–Rideal step for the reaction of gaseous CO with surface oxygen species of PdO to form CO_2. An activation energy of 9.2 kJ/mol was estimated for this reaction step. In addition, an apparent rate constant k_2^{app} (s^{-1}) was estimated for the process of back-spillover of oxygen. The ratio of the two rate constants (k_1/k_2^{app}) was found to be greater than 100 in the 500–700 °C range. A Langmuir–Hinshelwood surface elementary reaction step of adsorbed CO with atomic oxygen of PdO failed to describe the experimental transient kinetics of CO oxidation in the 500–700 °C range. The results of the present work provide the means for a better understanding of the effects of various additives and contaminants present in a three-way commercial catalytic converter and other related model catalysts on their OSC kinetic behavior. In addition, intrinsic effects of a given regeneration method for a commercial three-way catalyst on the OSC phenomenon could better be studied by making use of the results of the present mathematical model.
© 2003 Elsevier Inc. All rights reserved.

Keywords: Oxygen storage capacity; Three-way catalysts; Supported-Pd; Transient CO oxidation; Mathematical modeling of OSC; Pulse CO oxidation

1. Introduction

The oxygen storage capacity (OSC) of ceria and more recently of solid solutions of ceria–zirconia has been established to be a key parameter for the appropriate catalytic performance of commercial three-way catalysts (TWC) [1–8]. Yao and Yu Yao [5] first proposed the CO or H_2 pulse injection method that allows the measurement of the oxygen storage capacity of catalytic materials related to the TWC technology, which has been adopted by many researchers afterward [4,8–13]. Yao and Yu Yao [5] have proposed the distinction of two different oxygen storage capacities according to their developed method of measurement:

- The OSC (oxygen storage capacity, μatoms of O/g) related to the more reactive oxygen species and the most readily available oxygen atoms;
- The OSCC (oxygen storage capacity complete, μatoms of O/g) related to the total or maximum oxygen storage capacity under the applied experimental conditions.

The exact experimental protocol and possible reactions that may occur during the measurement of the OSC by CO pulses have been discussed [5,14].

Despite the extended use of the CO pulse injection method to quantify the OSC phenomenon, no attempts have yet been made toward the modeling of the pulse transient

* Corresponding author.
E-mail address: efstath@ucy.ac.cy (A.M. Efstathiou).

0021-9517/$ – see front matter © 2003 Elsevier Inc. All rights reserved.
doi:10.1016/S0021-9517(03)00151-9

response of CO obtained during the experiment. Such a modeling could allow the estimation of the transient rate of back-spillover of the oxygen process from ceria to the PM (Pt, Rh, Pd) surface and also of the rate of oxidation of CO to CO_2 on the PM surface. Knowledge of these two transient rates must be considered as highly desirable since the various oxygen storage materials must be correctly evaluated based not only on the amount of oxygen they can store but also on their intrinsic property of rate by which their stored surface/subsurface oxygen species can migrate from ceria to the metal/metal oxide surface. The role of the various additives and contaminants of commercial TWCs on the OSC could be better understood if their dependence on the quantity of stored oxygen and the relative rates of back-spillover of oxygen and oxidation of CO and HC on the supported metal surface are known. In addition, any evaluation of vehicle-aged TWC activity following a given regeneration method could be facilitated by knowing beforehand the improvement made in the rate of back-spillover of oxygen.

In the present work, it is demonstrated for the first time that the transient response of CO obtained after applying the pulse injection method for measuring the OSC phenomenon on a 1 wt% Pd/CeO_2 catalyst can be modeled very well via a two-step kinetic scheme which allows the evaluation of the transient rates of back-spillover of oxygen from ceria to the pre-oxidized Pd surface and also of the rate of oxidation of CO to CO_2 on the oxidized Pd surface. The dynamic mathematical modeling performed allows also the evaluation of the intrinsic rate constant, k (s^{-1}), associated with the elementary step of CO oxidation and of the apparent rate constant, k^{app} (s^{-1}), associated with the process of back-spillover of oxygen from ceria to the oxidized Pd surface. The results of this work have shown that the rate of back-spillover of oxygen is smaller by a factor ranging between 1.2 and 15 during the 8-s duration of the transient CO oxidation reaction in the 500–700 °C range.

A deeper understanding of the effects of crystal size and morphology of ceria and PM (Pt, Rh, Pd) metal on the transient rate of the very important process of back-spillover of oxygen over catalytic systems of technological importance can be obtained by the present proposed mathematical model.

2. Experimental

2.1. Apparatus for transient studies and the CSTR microreactor used

The pulse injection method for the measurement of OSC was performed on a transient flow system described elsewhere [15] using a CSTR microreactor (1.5-ml nominal volume) made of quartz. The basic design features of the reactor are given in Fig. 1. Its behavior as a single CSTR was verified following the procedures described in detail elsewhere [16,17]. The concepts used by Stockwell et al. [16] for the design of a CSTR microreactor made of stainless steel have been adopted. Local mixing of the gas entering the space above the very shallow catalyst bed (0.5 mg of Pd/CeO_2 catalyst plus 49.5 mg of SiO_2 in particle form, $d < 0.1$ mm) was achieved by drilling several holes on a quartz disk off-center to the entrance flow (see Fig. 1). Heating was provided by a small furnace (235-mm total length) where the reactor was horizontally placed.

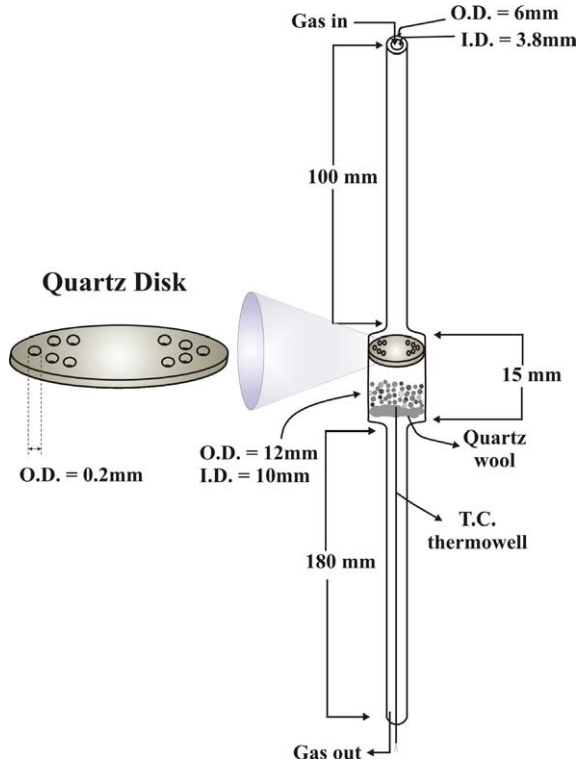

Fig. 1. Design features of the CSTR microreactor used for CO pulse injection experiments to model the OSC phenomenon.

2.2. Catalyst preparation and characterization

The 1 wt% Pd/CeO_2 catalyst was prepared by the wet impregnation method using the $Pd(NO_3)_2$ (Aldrich) precursor. The CeO_2 support (Aldrich) used was of standard grade (99.9% purity). After impregnation and drying (overnight at 120 °C), the catalyst sample was calcined in air at 400 °C for 2 h prior to use. The specific surface area of the support material was checked by N_2 adsorption at 77 K (BET method), using a Micromeritics 2100E Accusorb Instrument, and it was found to be 16 $m^2\,g^{-1}$. The dispersion of Pd in the supported catalyst was determined by H_2 chemisorption followed by TPD in He flow. In particular, after calcination of the sample at 500 °C for 2 h in a 20% O_2/He gas mixture, followed by H_2 (1 atm) reduction at 300 °C for 2 h, the feed was changed to He at 300 °C for 30 min to desorb any hydrogen chemisorbed on the Pd surface and the CeO_2 support (possible hydrogen spillover). The temperature was then increased to 500 °C in He flow and the sample was kept at 500 °C until no other hydrogen desorption was observed. The reactor was then cooled quickly in He flow to 25 °C and

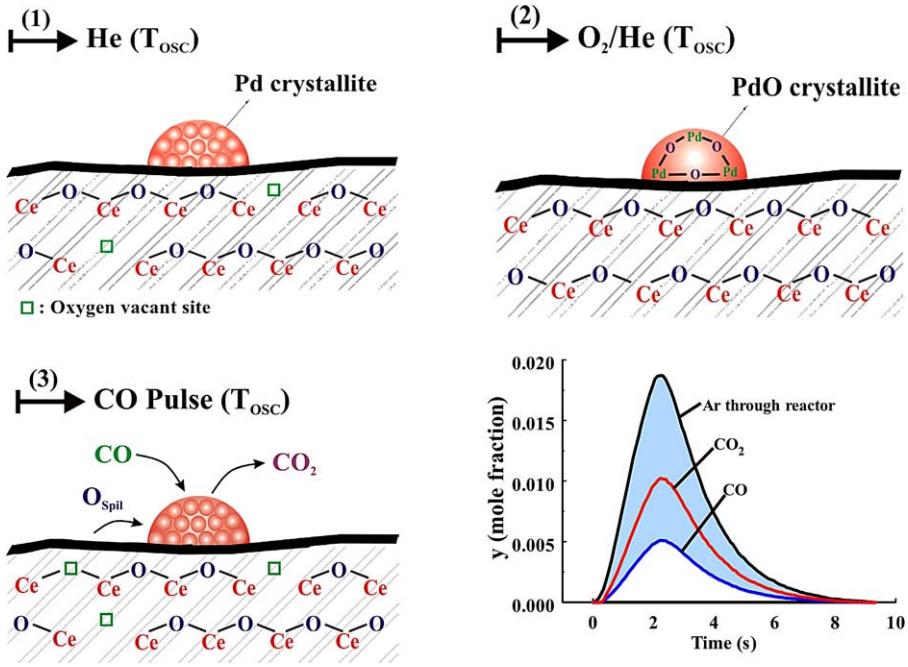

Fig. 2. Schematic representation of the effects of gas treatment during the sequence of steps 1–3 in performing the CO pulse injection experiment on the chemical structure and composition of 1 wt% Pd/CeO_2 catalyst. The transient response curves of CO and CO_2 obtained during step 3 are also shown. The shaded area between the Ar and CO response curves provides the amount of CO consumed or, equivalently, the oxygen storage capacity, OSC.

the feed was changed to a 1% H_2/He mixture for 30 min. It is noted that hydrogen chemisorption from the indicated gas mixture eliminates the possibility of palladium hydride formation [18]. Following this chemisorption step, the feed was changed back to He to carry out a TPD experiment. From the amount of hydrogen desorbed during TPD and the amount of Pd in the sample, the dispersion of Pd was estimated to be 61.5% (57.7 μmol/g). Calcination of the Pd/CeO_2 fresh sample at 700 °C in a 20% O_2/He gas mixture, followed by H_2 (1 atm) reduction at 300 °C for 2 h and the same further treatment in He flow and H_2 chemisorption/TPD as previously mentioned, resulted in a 54% metal dispersion.

TEM measurements performed on the same Pd/CeO_2 catalyst (following calcination in air at 500 °C for 1 h and H_2 reduction at 300 °C) provided an average Pd particle size of about 2.0 nm (±0.1 nm). Considering a spherical particle geometry and using the formula [19], D (%) = $1.1/d$ (nm) × 100, a value of 55% for metal dispersion was calculated. Note the good agreement in D (%) provided by the TEM and H_2 chemisorption measurements. TEM studies were performed after dispersing 5 mg of powder sample in 1 ml of ethanol/water mixture (1:1) kept in an ultrasonic bath for 2 h followed by deposition on a carbon-covered copper grid and drying at 25 °C. The instrument used was a JEOL 1010 electron microscope operated at an acceleration voltage of 80 kV.

2.3. CO pulse injection experiments for OSC measurements

The catalyst sample was pretreated in 20% O_2/He for 2 h at 500 °C followed by H_2 (1 atm) for 2 h at 300 °C before all CO pulse injection experiments. The 50-mg catalyst sample used (0.5 mg of Pd/CeO_2 + 49.5 mg of SiO_2) was prepared as follows. Ten milligrams of Pd/CeO_2 catalyst was weighted and thoroughly mixed with 990 mg of SiO_2. From the resulting solid mixture, 50 mg was weighted and placed in the catalytic microreactor.

The experimental protocol followed for the measurement of OSC is illustrated schematically in Fig. 2.

- *Step 1*: After its pretreatment, the catalyst sample was brought into He flow at the temperature (T_{OSC}) the OSC would be measured. At this point, the Pd is in its fully reduced state, while ceria exposes oxygen vacant sites.
- *Step 2*: The catalyst was then treated in a mixture of 20% O_2/He at T_{OSC} for 1 h. T_{OSC} varied in the 450–700 °C range in which Pd crystallites were oxidized into PdO, as indicated by in situ SEM and TPR studies [20–23]. At the same time, oxygen is adsorbed onto ceria via direct gas-phase chemisorption [24,25] and probably also by oxygen spillover from the metal to the ceria surface [26].
- *Step 3*: After a 2-min flush of reactor in He flow, a CO pulse (1.0 μmol) was directed into the reactor. During this pulse, surface oxygen species associated with PdO and oxygen from ceria (surface/subsurface) are reacted off by CO, giving CO_2 as a gas product. The mechanism by which this transient kinetics of CO oxidation occurs is described in the following section.

The CO and CO_2 gas-phase dynamic responses obtained from the last experimental step 3 were followed continuously by an *online* mass spectrometer. These responses are

shown in Fig. 2. The Ar response represents the dynamics of a nonadsorbing and nonreacting gas when pulsed (same amount as the CO) through the reactor with the catalyst present. The area difference between the Ar and the CO responses allows the estimation of the amount of CO consumed during the pulse experiment. In addition, integration of the CO_2 transient response yields the amount of CO_2 produced. If no other side reactions occur, the amount of OSC (μatoms of O/g) reflects either the amount of CO consumed or that of CO_2 produced. Intraparticle mass-transfer resistances during the CO pulse experiments in the 500–700 °C range have proven to be negligible according to the criteria proposed in the literature [27]. External mass transfer resistances based on the catalyst particle were also proven to be negligible as described in the following Section 4.1.

The dynamic gaseous responses obtained by mass spectrometry were calibrated against standard mixtures. The mass numbers (m/z) 28, 40, and 44 were used for CO, Ar, and CO_2, respectively. The cracking coefficient, cc (28/44), which is the ratio of the mass spectrometer signal at $m/z = 28$ to that at $m/z = 44$ for the CO_2 molecular species, was measured from a standard CO_2/He gas mixture. This coefficient is needed for the quantification of the CO signal. The concentration of CO in the input pulse and the amount of catalyst used for the OSC experiments (0.3–0.5 mg of Pd/CeO_2 diluted in SiO_2) were carefully chosen to achieve CO conversions lower than 20%. The total flow rate of the carrier gas (He) was kept constant at 100 scc/min.

3. Mathematical modeling

In this section, a mathematical model is developed which describes the dynamic response of the gaseous CO observed during the pulse transient experiment.

3.1. Kinetic model of the CO oxidation reaction in the 500–700 °C range

Two reaction mechanisms have been considered for the transient CO oxidation reaction, i.e., the Eley–Rideal and the Langmuir–Hinshelwood. These reaction mechanisms will be tested against the calculated pulse transient response and other features of the pulse transient experiment.

3.1.1. Eley–Rideal mechanism

A transient kinetic model describing the chemical processes under consideration is based on the following two mechanistic steps:

$$\mathrm{CO(g)} + \mathrm{O\text{–}S_1} \xrightarrow{k_1} \mathrm{CO_2(g)} + \mathrm{S_1}, \qquad \text{(step 1)}$$

$$\mathrm{O\text{–}S_2} + \mathrm{S_1} \xrightarrow{k_2^{\mathrm{app}}} \mathrm{O\text{–}S_1} + \mathrm{S_2}, \qquad \text{(step 2)}$$

where S_1 denotes an oxygen vacant adsorption site on the PdO surface, as discussed in Section 2.3 and shown in Fig. 2, S_2 denotes a site on ceria with which an adsorbed oxygen and/or lattice oxygen species is associated, k_1 is the intrinsic rate constant of elementary step 1 of the CO oxidation reaction, and k_2^{app} is an apparent rate constant associated with the kinetics of the back-spillover of the oxygen process from ceria to the surface of PdO.

Elementary reaction step 1 is of the Eley–Rideal (ER) type mechanism. The choice of this mechanism was made based on three observations. First, the initial state of the Pd surface is that of palladium oxide and not of a fully covered Pd surface by chemisorbed oxygen, as explained in Section 2.3. Thus, chemisorption of CO cannot take place on the surface of PdO, at least in the initial period of the pulse experiment. Second, during the course of the transient CO oxidation reaction, oxygen from ceria is transferred onto the surface of PdO/Pd with comparable rates to those of oxygen removal (by CO reduction) from the PdO phase, according to the present results (Fig. 6). Thus, chemisorbed CO onto an oxidized Pd state may not be expected to be formed in the 500–700 °C range. Third, in situ DRIFTS studies performed in this work have revealed no molecularly chemisorbed CO in the 500–700 °C range over the catalyst after the first pulse of CO on the PdO/CeO_2 surface.

It is important to mention here that the direct reaction of gas-phase CO with oxygen species on CeO_2 support in the 500–700 °C range was not considered because the same experiments performed with 0.5 mg of CeO_2 (diluted in 49.5 mg of SiO_2) resulted in less than 12% of the OSC measured over the 0.5-mg Pd/CeO_2 catalyst sample. More precisely, the amounts of 12.1, 21.4, and 35.3 μmol of CO_2/g (or μatoms of O/g) were measured at 500, 600, and 700 °C, respectively. In addition, these measurements revealed that no uptake of chemisorbed CO on CeO_2 alone occurred during the pulse experiment in the 500–700 °C range.

3.1.2. Langmuir–Hinshelwood mechanism

If the CO oxidation reaction on the present PdO/CeO_2 catalytic system in the 500–700 °C range proceeds by a Langmuir–Hinshelwood (LH) mechanism, the appropriate elementary reaction steps are as follows:

$$\mathrm{CO(g)} + \mathrm{S_1} \underset{k_\mathrm{d}}{\overset{k_\mathrm{a}}{\rightleftarrows}} \mathrm{CO\text{–}S_1}, \quad \frac{k_\mathrm{d}}{k_\mathrm{a}} = K, \qquad \text{(step 3)}$$

$$\mathrm{CO\text{–}S_1} + \mathrm{O\text{–}S_1} \xrightarrow{k_4} \mathrm{CO_2(g)} + 2\mathrm{S_1}, \qquad \text{(step 4)}$$

$$\mathrm{O\text{–}S_2} + \mathrm{S_1} \xrightarrow{k_2^{\mathrm{app}}} \mathrm{O\text{–}S_1} + \mathrm{S_2}. \qquad \text{(step 2)}$$

In the proposed mathematical model, step 3 is considered to be in equilibrium. Chemisorption of CO is considered to proceed on the surface oxygen vacant sites (□) or the Pd/□ pair sites present in the PdO phase.

3.2. Unsteady-state mass balances

The mass balances for the two adsorbed $O\text{–}S_1$ and $O\text{–}S_2$ species in the case of the Eley–Rideal mechanism for the CO

oxidation reaction are given by

$O\text{–}S_1$:

$$\frac{dN_{O\text{–}S_1}}{dt} = -k_1 y_{CO}\frac{N_{O\text{–}S_1}}{N^0_{O\text{–}S_1}} + k_2^{app}\left(1 - \frac{N_{O\text{–}S_1}}{N^0_{O\text{–}S_1}}\right)N_{O\text{–}S_2} \quad (1)$$

$$\left(t = 0,\ N_{O\text{–}S_1} = N^0_{O\text{–}S_1}\right)$$

$O\text{–}S_2$:

$$\frac{dN_{O\text{–}S_2}}{dt} = -k_2^{app}\left(1 - \frac{N_{O\text{–}S_1}}{N^0_{O\text{–}S_1}}\right)N_{O\text{–}S_2} \quad (2)$$

$$\left(t = 0,\ N_{O\text{–}S_2} = N^0_{O\text{–}S_2}\right).$$

The mass balances in the case of the Langmuir–Hinshelwood mechanism are as follows:

$O\text{–}S_1$:

$$\frac{dN_{O\text{–}S_1}}{dt} = -k_4\theta_{CO}N_{O\text{–}S_1} + k_2^{app}\left(1 - \theta_{CO} - \frac{N_{O\text{–}S_1}}{N^0_{O\text{–}S_1}}\right)N_{O\text{–}S_2} \quad (3)$$

$$\left(t = 0,\ N_{O\text{–}S_1} = N^0_{O\text{–}S_1},\ \text{and } \theta_{CO} = 0\right),$$

$O\text{–}S_2$:

$$\frac{dN_{O\text{–}S_2}}{dt} = -k_2^{app}\left(1 - \theta_{CO} - \frac{N_{O\text{–}S_1}}{N^0_{O\text{–}S_1}}\right)N_{O\text{–}S_2} \quad (4)$$

$$\left(t = 0,\ N_{O\text{–}S_2} = N^0_{O\text{–}S_2}\right).$$

The mass balance for the gaseous CO species in the CSTR microreactor is given by

$$N_T\frac{dy_{CO}}{dt} = F_T y^{in}_{CO} - F_T y_{CO} - k_1 y_{CO} N_{O\text{–}S_1} W_{cat} \quad (5)$$

$$(t = 0,\ y_{CO} = 0)$$

in the case of the Eley–Rideal mechanism and by

$$N_T\frac{dy_{CO}}{dt} = F_T y^{in}_{CO} - F_T y_{CO} - \left(k_a y_{CO}\left(1 - \theta_{CO} - \frac{N_{O\text{–}S_1}}{N^0_{O\text{–}S_1}}\right) - k_d\theta_{CO}\right) \times N^0_{O\text{–}S_1} W_{cat} \quad (6)$$

$$(t = 0,\ y_{CO} = 0,\ \theta_{CO} = 0),$$

in the case of the Langmuir–Hinshelwood mechanism.

The definitions and units of all parameters that appear in Eqs. (1)–(6) are given in Table 1.

The total number of moles (N_T) in the gas phase of the CSTR microreactor that appears in the mass balances of Eqs. (5) and (6) was estimated by employing the ideal-gas law and using the gas-phase volume of the CSTR reactor with the catalyst bed in place. The latter quantity was estimated by means of the simulated transient response of Ar gas following the switch from He to 5% Ar/He gas mixture bypass and through the reactor [16,17] and was found to be 0.5 cm^3. The value of $N^0_{O\text{–}S_1}$ parameter is taken as that corresponding to the metal dispersion (the number of surface Pd atoms per gram of catalyst is assumed to remain the same for the Pd and PdO supported phases).

Table 1
Definition of parameters used in the mathematical model

Parameter	Definition	Units
k_1	Kinetic rate constant of reaction step 1	s^{-1}
k_2^{app}	Kinetic rate constant of reaction step 2	s^{-1}
k_a	Kinetic rate constant of CO adsorption (step 3)	s^{-1}
k_d	Kinetic rate constant of CO desorption (step 3)	s^{-1}
k_4	Kinetic rate constant associated to reaction step 4	s^{-1}
y_{CO}	CO output mole fraction	mol%
$y_{CO,max}$	Maximum CO output mole fraction	mol%
y^{in}_{CO}	CO input mole fraction	mol%
$N_{O\text{–}S_1}$	Amount of adsorbed oxygen on Pd surface	μatom/g
$N^0_{O\text{–}S_1}$	Initial ($t = 0$) amount of adsorbed oxygen on Pd surface	μatom/g
$N_{O\text{–}S_2}$	Amount of adsorbed oxygen on cerium oxide	μatom/g
$N^0_{O\text{–}S_2}$	initial ($t = 0$) amount of adsorbed oxygen on cerium oxide	μatom/g
θ_{CO}	Surface coverage of adsorbed CO in the Pd surface	
F_T	Total molecular flow	μmol/s
N_T	Total number of moles in the gas phase	μmol
W_{cat}	Catalyst mass	g

3.3. Input y^{in}_{CO} function

The function describing the input pulse $y^{in}_{CO}(t)$ in the pulse dynamic experiment that appears in the mass balances of Eqs. (5) and (6) was obtained by fitting the experimentally measured pulse of Ar (1 μmol) after directed bypass of the reactor (see Section 2.3 and Refs. [16,17]. As shown in Fig. 3, this pulse is described very well by the following equation with a correlation factor $R = 0.9992$,

$$Z = a e^{a_1(t-t_1)^4} + a_2 e^{a_3(t-t_2)^2} + a_4 e^{a_5(t-t_3)^2}, \quad (7)$$

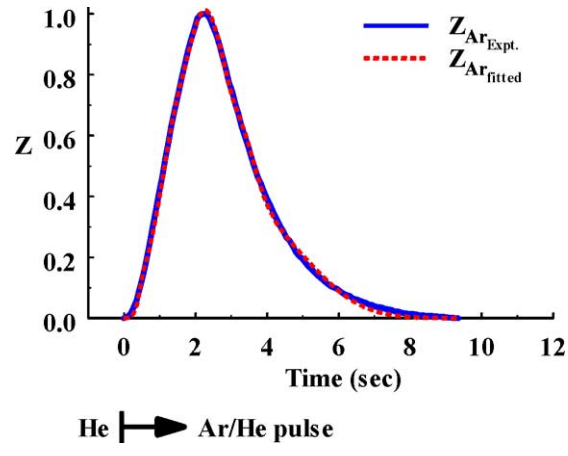

Fig. 3. Experimental and fitted (Eq. (7)) dimensionless pulse transient response of Ar obtained bypass the reactor according to the switch He → Ar/He pulse (1.0 μmol).

Table 2
Simulated parameter values of the input pulse response curve based on Eq. (7)

Parameter	Value	Std. dev. error (%)
a	0.1089	1.3
a_1	−0.5462	4.3
a_2	0.7979	2.9
a_3	−0.2887	2.9
a_4	0.2517	1.3
a_5	−0.1396	1.4
t_1	2.5637	1.1
t_2	3.6242	1.7
t_3	5.5737	13.3

where

$$Z = \frac{y_{\mathrm{Ar}}^{\mathrm{in}}(t)}{y_{\mathrm{Ar}}^{\mathrm{max}}}, \quad 0 \leqslant Z(t) \leqslant 1. \tag{8}$$

The optimum fitting parameters a, a_1–a_5, and t_1–t_3 are tabulated in Table 2.

3.4. Optimization of k_1 and k_2^{app}

The finite-difference method (fully implicit scheme) was used for the solution of the coupled differential Eqs. (1), (2), and (5), in the case of the ER mechanism. The simulation of the experimental CO pulse transient response obtained during the OSC measurement on the 1 wt% Pd/CeO_2 catalyst was based on the following three criteria.

1st Criterion. The maximization of the correlation factor ($\Re$) between the simulated and experimental gas-phase CO concentration values according to

$$\Re = \frac{n(\sum XY) - (\sum X) - (\sum Y)}{\sqrt{[n\sum X^2 - (\sum X)^2] \cdot [n\sum Y^2 - (\sum Y)^2]}}, \tag{9}$$

where X and Y are respectively the simulated and the experimental values of gas-phase CO concentration (y_{CO}) and n is the number of experimental values of CO concentration (y_{CO}).

2nd Criterion. The predicted values of $N_{\mathrm{O-S_1}}$ and $N_{\mathrm{O-S_2}}$ should be vanishing (e.g., less than 2%) by the end of the CO pulse:

$$N_{\mathrm{O-S_1}} \to 0 \quad \text{and} \quad N_{\mathrm{O-S_2}} \to 0. \tag{10}$$

3rd Criterion. The predicted values of $N^0_{\mathrm{O-S_1}}$ and $N^0_{\mathrm{O-S_2}}$ must agree, within a 2% tolerance, with the corresponding experimental values:

$$N^0_{\mathrm{O-S_1}} + N^0_{\mathrm{O-S_2}} = \int R_{\mathrm{COoxid.}}\,\mathrm{d}t, \tag{11}$$

$$N^0_{\mathrm{O-S_2}} = \int R_{\mathrm{spillover}}\,\mathrm{d}t, \tag{12}$$

$$N^0_{\mathrm{O-S_1}} + N^0_{\mathrm{O-S_2}} = N_{\mathrm{COconsumed}} \tag{13}$$

(determined by the experiment).

The rate expressions of CO oxidation, $R_{\mathrm{COoxid.}}$, and back-spillover of the oxygen process, $R_{\mathrm{spillover}}$, are given in the following Section 3.5.

For a more efficient determination of the optimum values of the two rate constants, k_1 and k_2^{app}, the above three criteria have been combined by means of a single parameter Ω,

$$\Omega = \Re \cdot \left(\frac{N^0_{\mathrm{O-S_1}} - N^{t_{\mathrm{f}}}_{\mathrm{O-S_1}}}{N^0_{\mathrm{O-S_1}}}\right) \cdot \left(1 - \frac{|N^0_{\mathrm{O-S_2}} - \int_0^{t_{\mathrm{f}}} R_{\mathrm{COspillover}}|}{N^0_{\mathrm{O-S_2}}}\right), \tag{14}$$

where t_{f} is the final time during the CO pulse transient experiment at which y_{CO} is practically zero. Optimum values of k_1 and k_2^{app} should maximize Ω (close to unity).

3.5. Rates of CO oxidation and back-spillover of the oxygen process

In the case of the ER mechanism, the rates of CO oxidation (step 1) and of back-spillover of the oxygen process (step 2) are respectively given by

$$R_{\mathrm{COoxid.}}(\mathrm{ER}) = k_1 y_{\mathrm{CO}} N_{\mathrm{O-S_1}} \quad (\mu\mathrm{mol\ of\ O/(g\,s)}), \tag{15}$$

$$R_{\mathrm{spillover}} = k_2^{\mathrm{app}} N_{\mathrm{O-S_2}}(1 - N_{\mathrm{O-S_1}}/N_{\mathrm{O-S_2}}) \quad (\mu\mathrm{mol\ of\ O/(g\,s)}). \tag{16}$$

In the case of the Langmuir–Hinshelwood mechanism, the rate of CO oxidation (step 4) is given by

$$R_{\mathrm{COoxid.}}(\mathrm{LH}) = k_4 \theta_{\mathrm{CO}} N_{\mathrm{O-S_1}} \quad (\mu\mathrm{mol\ of\ O/(g\,s)}). \tag{17}$$

4. Results and discussion

4.1. External mass-transfer considerations

It is very important to consider whether the pulse transient kinetic experiments performed were conducted under conditions where the external mass transport rate, that from the gas phase to the external surface of the catalyst particle was large enough, so only kinetic rates were measured in the high temperature range of 500–700 °C. The rate of external mass transfer (r_{p}) can be estimated according to the following relationship [27]:

$$r_{\mathrm{p}} = k_{\mathrm{g}} a_{\mathrm{m}} (C_{\mathrm{b}} - C_{\mathrm{s}}), \tag{18}$$

where, k_{g} is the mass-transfer coefficient (m/s), a_{m} is the specific external surface of the solid catalyst particle ($\mathrm{m^2/g}$), C_{b} is the concentration of CO in the bulk gas phase ($\mathrm{mol/m^3}$), and C_{s} is the concentration of CO ($\mathrm{mol/m^3}$) in the gas phase very close to the external surface of the catalyst particle.

In the case where $C_{\mathrm{b}} - C_{\mathrm{s}} = 5\%\ C_{\mathrm{b}}$, and when the latter is considered as a sufficient criterion for the absence of external mass transfer resistances, then according to Eq. (18) and the data presented in Table 3 the rate of external mass transfer at 600 °C was calculated to be

Table 3
Parameter values for the estimation of external mass-transfer resistance for the CO pulse experiment at 600 °C

Parameter	Value
Schmidt number (*Sc*)	0.90
Mass flux (G)	2×10^{-2} kg/(m^2 s)
Reynolds number (Re)$_p$	0.033
Mass-transfer coefficient (k_g)	1.2×10^{-1} m/s
External surface of the solid catalyst particle (a_m)	0.6 m^2/g
Catalyst particle size (d_p)[a]	0.06 mm
Maximum concentration of CO in the input pulse ($y_{CO,max}$)	1.87 mol%
Total pressure (P_T)	1 atm

[a] Based on an optical microscope, where it was found that the size of catalyst particles was in the range of 0.01–0.15 mm with an approximate average size of 0.06 mm.

940 $\mu mol_{CO}/(g\,s)$. As will be shown in the following Section 4.4 (Fig. 6b), the maximum experimental value of the CO oxidation reaction rate at 600 °C was estimated to be about 90 $\mu mol_{CO}/(g\,s)$. This value is about 10 times smaller than the one calculated for the rate of external mass transfer. Thus, it can be stated that under the present experimental conditions external mass-transfer resistances are not significant.

4.2. Fitting of the gas-phase CO pulse transient response. Eley–Rideal mechanism for the CO oxidation reaction

Fig. 4 presents the experimental CO output pulse transient response curves obtained over the 1% Pd/CeO_2 catalyst at 500 and 600 °C as well as the corresponding simulation curves. In the case of 500 °C (Fig. 4a), the agreement between the experimental and simulation curves is excellent. The correlation factor R is 0.9913, which fulfills very adequately the 1st criterion. The optimum values for the two rate constants are found to be $k_1 = 304.0\ s^{-1}$ and $k_2^{app} = 3.2\ s^{-1}$. In the case of 600 °C (Fig. 4b), the agreement between the experimental and the simulation results is also quite satisfactory ($R = 0.9894$), even though the simulation curve does not predict so accurately the peak maximum and the rising part of the pulse (first 2 s, Fig. 4a). The optimum values for the two rate constants are $k_1 = 359.0\ s^{-1}$ and $k_2^{app} = 3.9\ s^{-1}$. The experimental parameters used in both simulations and the resulting parameters calculated by the model are tabulated in Table 4. In this table, corresponding values at the highest temperature studied (700 °C) are also reported.

4.3. Transient evolution of $N_{O–S_1}$ and $N_{O–S_2}$

The proposed mathematical model also predicts the transient evolutions of the amounts of the two oxygen species in the two reservoirs, those of ceria ($N_{O–S_2}$) and PdO ($N_{O–S_1}$). Fig. 5 presents the transient behaviors of $N_{O–S_1}$ and $N_{O–S_2}$ during the CO oxidation reaction in the pulse transient experiments described in Fig. 4. It is clear that, for $t < t_{max}$,

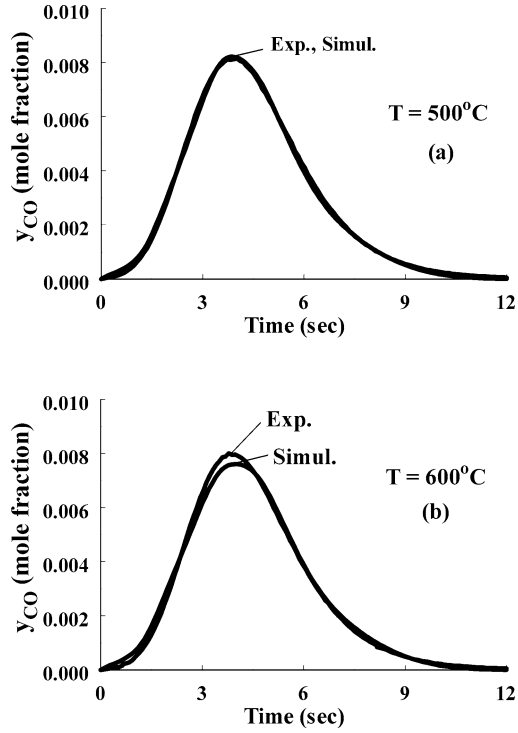

Fig. 4. Experimental and simulated pulse transient responses of gas-phase CO at the exit of the CSTR microreactor related to the OSC measurement at (a) 500 and (b) 600 °C over the 1 wt% Pd/CeO_2 catalyst.

Table 4
Experimental and simulated parameter values of the CO pulse transient response obtained at 500, 600, and 700 °C over the 1 wt% Pd/CeO_2 catalyst[a]

Parameter	Value		
	500 °C	600 °C	700 °C
$y_{CO,max}$ (mol%)	0.0187	0.0187	0.0187
$N^0_{O–S_1}$ (μatom/g)	58	58	58
F_T (μmol/s)	68.3	68.3	68.3
N_T (μmol)	4.0	3.5	3.1
W_{cat} (g)	0.0005	0.00035	0.00035
k_1 (s^{-1})	304.0	359.0	401.0
k_2^{app} (s^{-1})	3.2	3.9	4.1
$\Re$	0.9913	0.9894	0.9909
Ω	0.9907	0.9882	0.9896

[a] An Eley–Rideal mechanism is assumed for the CO oxidation reaction.

where t_{max} is the time of appearance of the maximum in the concentration of CO, the rate of change of $N_{O–S_1}$ is significantly lower than that of $N_{O–S_2}$. In particular, at 600 °C the amount of $N_{O–S_1}$ for $t \leqslant t_{max}$ remains practically constant (Fig. 5b). In addition, the rates of change of the amounts of the two oxygen species during the pulse are different and depend on the reaction temperature. The duration of the CO pulse is approximately 10 s. The values of $N_{O–S_1}$ at the end of the pulse ($t > 10$ s) at 500 and 600 °C are respectively 0.037 and 0.071, while the corresponding values of $N_{O–S_2}$ are 1.5×10^{-7} and 2.3×10^{-7}, respectively. Therefore, the 2nd criterion for the estimation of the optimum values of the two rate constants is also fulfilled.

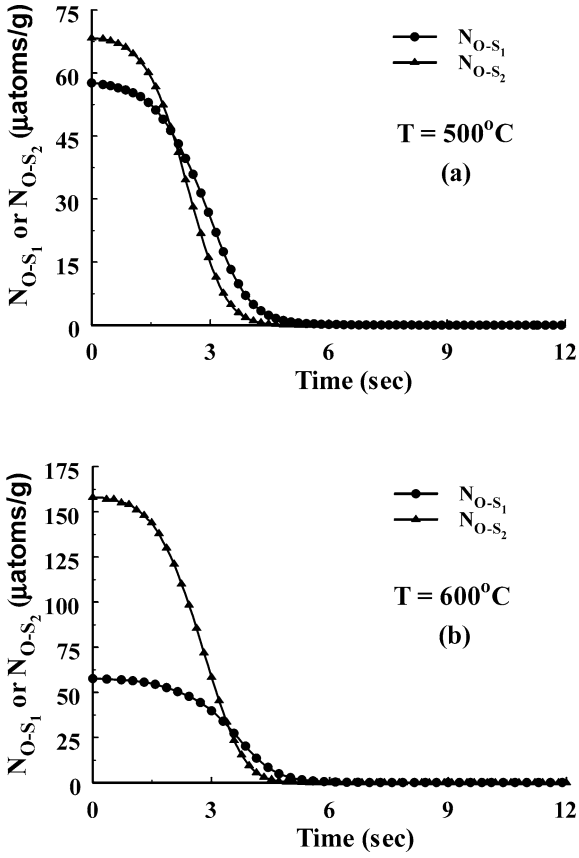

Fig. 5. Calculated transient response curves of $N_{O–S_1}$ and $N_{O–S_2}$ quantities based on the OSC measurements at (a) 500 and (b) 600 °C over the 1 wt% Pd/CeO_2 catalyst.

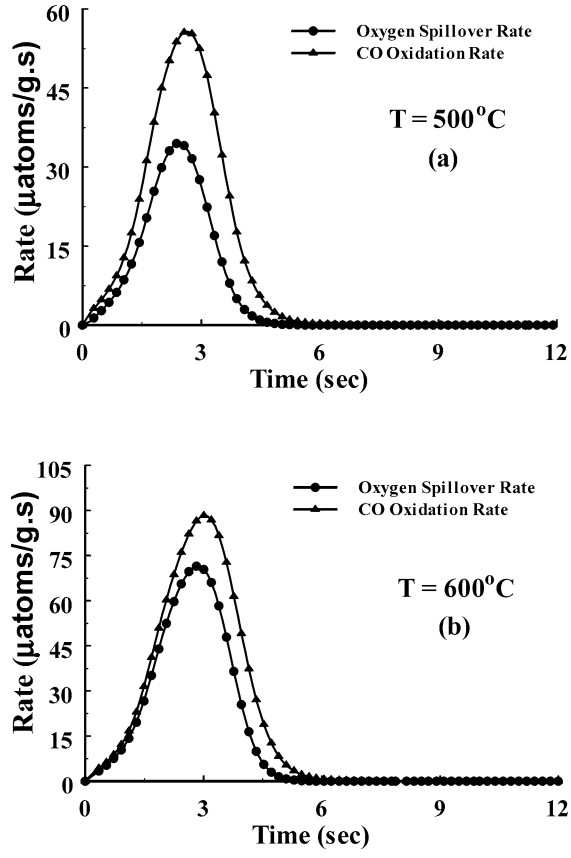

Fig. 6. Calculated transient response curves of the rate of CO oxidation and back-spillover of oxygen during OSC measurement at (a) 500 and (b) 600 °C over the 1 wt% Pd/CeO_2 catalyst.

4.4. *Transient rates for the CO oxidation and back-spillover of oxygen processes*

Fig. 6 presents the evolution of the rates of CO oxidation (step 1) and oxygen back-spillover (step 2) during the CO pulse transient experiment at 500 °C (Fig. 6a) and 600 °C (Fig. 6b). It should be pointed out that these transient rates *cannot be measured experimentally*. They can only be estimated by performing a kinetic/mathematical analysis of the CO pulse transient response as shown in the present work.

In Fig. 6b ($T = 600$ °C), it is observed that the CO oxidation reaction rate is similar to that of the oxygen back-spillover for reaction times less than 2 s and then becomes higher. In particular, at $t = 5$ s, the spillover rate is about 5 μatoms/(g s), while the value of the rate of CO oxidation is 30 μatoms/(g s). In the case of 500 °C (Fig. 6a), the rate value of back-spillover of oxygen is always significantly lower than that of the CO oxidation reaction.

Fig. 7 shows the ratio of the maximum rate of CO oxidation to the maximum rate of back-spillover of oxygen as a function of reaction temperature in the 500–700 °C range. As the reaction temperature increases from 500 to 700 °C, the transient rate of back-spillover of oxygen takes values approaching those of the rate of CO oxidation. At 700 °C, the maximum transient rate of CO oxidation on PdO is only about 20% higher than the maximum transient rate of back-spillover of oxygen. The results presented in Figs. 6 and 7 are indeed very significant since they illustrate for the first time, in this type of transient kinetics of CO oxidation, the relative importance of the two rates in the transient regime as a function of the reaction temperature.

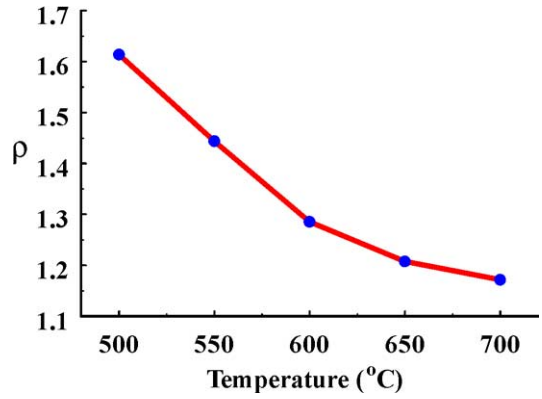

Fig. 7. Calculated temperature dependence of the ratio of the maximum transient rate of CO oxidation to that of back-spillover of oxygen obtained during the CO pulse injection experiment for measuring the OSC over the 1 wt% Pd/CeO_2 catalyst in the 500–700 °C range.

Vayenas and Pitselis [28] have proposed a mathematical model describing the NEMCA effect on porous conduc-

tive catalyst films on solid electrolyte supports. Their model accounts for the back-spillover of promoting anionic $O^{\delta-}$ species from the solid electrolyte onto the catalyst surface. The same type of model was then applied to describing the effect of metal–support interactions for the case of finely dispersed metal nanoparticles on ZrO_2- and TiO_2-based porous supports, where the same type of $O^{\delta-}$ back-spillover mechanism is operative. Vayenas and Pitselis [28] have concluded that, in the case of dispersed Pt-supported catalysts, the adsorbed O atom can migrate 1 μm/s on Pt at 400 °C. Unless the oxidation reaction TOF is higher than 10^3 s^{-1}, which is practically never the case, the $O^{\delta-}$ back-spillover double layer is present on the supported nanocrystalline metal particles. Their simulation results agree with ours, in the sense that the rate of back-spillover of oxygen species is significant with respect to the CO oxidation rate.

Let us discuss the transient behavior of the two rates presented in Fig. 6. As soon as the gaseous CO species reach the entrance of the shallow catalyst bed, diffusion of CO into the pore system of CeO_2 particles is very rapid and the CO oxidation reaction on the pre-oxidized Pd (PdO phase) supported within the pore system of ceria is rapidly initiated. At the same time, due to the fact that oxygen vacant sites are created by the CO oxidation reaction on the PdO phase, ceria begins to supply oxygen species to the surface of PdO via a back-spillover mechanism. At this point it should be clarified that subsurface oxygen of PdO could also be transferred to the surface of PdO. However, its amount is very small compared to that of oxygen stored on CeO_2. As the reaction proceeds, the oxygen pool in ceria begins to evacuate and thus the spillover rate is reduced. A maximum in the rate of consumption of CO (or CO_2 production) occurs when the product $y_{CO} \times N_{O-S_1}$ is maximized (see Eq. (15)). Finally, the spillover rate is reduced significantly when the oxygen pool in ceria is largely reduced (e.g., at $t = 5$ s, $T = 600$ °C). In contrast, the CO oxidation reaction continues since oxygen is still available on the PdO surface and CO is available in the gas phase (CO pulse duration is 10 s).

Integration of the curves of the transient rates (Fig. 6) leads to the calculation of the initial amount of adsorbed oxygen in each pool, i.e., that of PdO ($N^0_{O-S_1}$) and of ceria ($N^0_{O-S_2}$). The estimated and experimental values of $N^0_{O-S_1}$ and $N^0_{O-S_2}$ are reported in Table 5 for the CO pulse experiments performed in the 500–700 °C range. It is noted that

Table 5
Experimental and simulated values of $N^0_{O-S_1}$ and $N^0_{O-S_2}$ based on the mathematical modeling of the CO transient pulse response in the 500–700 °C range according to the Eley–Rideal mechanism

Temperature	Experimental (μatom/g)		Simulated (μatom/g)	
(°C)	$N^0_{O-S_1}$	$N^0_{O-S_2}$	$N^0_{O-S_1}$	$N^0_{O-S_2}$
500	58.0	67.3	58.0	67.3
550	58.0	92.2	58.0	92.3
600	58.0	158.0	58.0	157.4
650	58.0	186.9	58.0	186.7
700	58.0	206.4	58.0	206.5

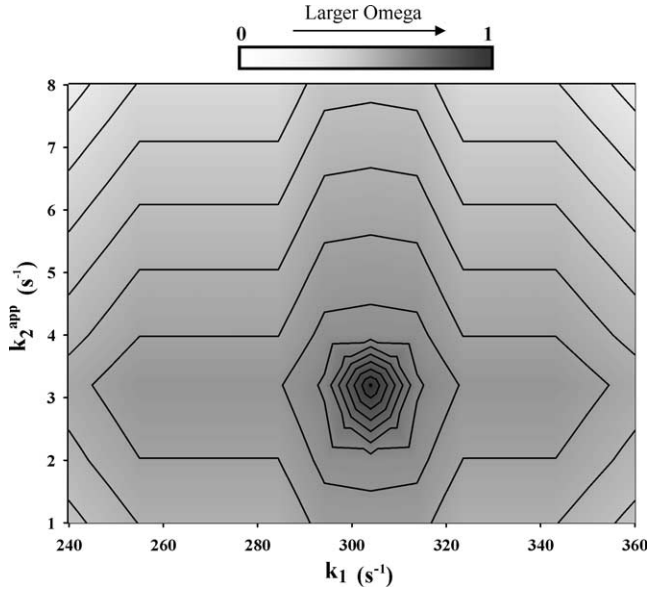

Fig. 8. Contour diagram of k_1 vs k_2^{app}. Simulation results correspond to experimental results of the CO pulse injection experiment performed at 500 °C over the 1 wt% Pd/CeO_2 catalyst.

the 3rd criterion is satisfied very well since the predicted values of $N^0_{O-S_1}$ and $N^0_{O-S_2}$ are in excellent agreement with the experimental ones at all reaction temperatures studied.

4.5. Optimization of k_1 and k_2^{app}

To find the optimum values of the rate constants of the CO oxidation and oxygen back-spillover reaction processes, a series of simulations with the values of k_1 and k_2^{app} in the 1 to 1000 s^{-1} range were carried out. The goal was to search for those k values maximizing the parameter Ω given by Eq. (14). Fig. 8 presents a contour diagram of k_1 vs k_2^{app} in the case of the CO pulse injection experiment at 500 °C (see Figs. 4a–6a). In Fig. 8, the darker gray color indicates larger values of the Ω parameter. The solid lines signify the borders between areas of changing color shading, thus a change in the range of Ω values. As shown in Fig. 8, the parameter Ω is maximized when $k_1 = 304$ s^{-1} and $k_2^{app} = 3.2$ s^{-1}. The value of Ω for this set of optimum k's is 0.9907.

The optimum values of k_1 for the CO pulse transient experiments performed in the 500–700 °C range were used to obtain the intrinsic activation energy of the Eley–Rideal mechanism of CO oxidation to CO_2 (step 1). The corresponding Arrhenius plot shown in Fig. 9 yields an activation energy of 9.2 ± 0.1 kJ/mol and a pre-exponential factor of 1200 ± 5 s^{-1} with $R = 0.99$.

4.6. Fitting of the gas-phase CO pulse transient response

Langmuir–Hinshelwood mechanism for the CO oxidation reaction

The modeling of the experimental CO pulse transient responses shown in Fig. 4 using the Langmuir–Hinshelwood

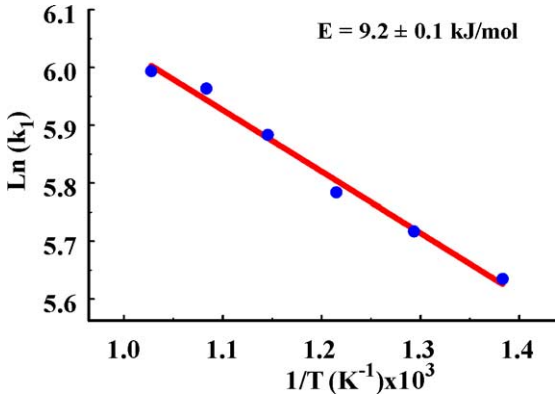

Fig. 9. Arrhenius plot of Ln(k_1) vs $1/T$ for the determination of the intrinsic activation energy of the Eley–Rideal mechanism of CO oxidation on PdO/CeO_2 catalyst in the 500–700 °C range during the OSC measurements.

mechanism has been performed by varying the four kinetic rate constants, k_d, k_a, k_4, and k_2^{app} (that appear in the corresponding reaction scheme described by steps 2–4 of Section 3.1.2) and using the appropriate material balance equations (Eqs. (3), (4), and (6) of Section 3.2). To avoid the simultaneous evaluation of all the above-mentioned kinetic rate constants by just fitting the single experimental CO response curve, the rate constants for CO adsorption (k_a) and desorption (k_d) were calculated separately, using experimental data provided in the literature. The rate constant for CO adsorption was calculated using the following expression suggested in Ref. [29]:

$$k_a = S_0\sigma\left(\frac{R}{2\pi M}\right)^{0.5}\left(\frac{P_T}{R}\right)N_A\left(\frac{1}{T}\right)^{0.5}, \tag{19}$$

where S_0 is the sticking coefficient, σ is the surface metal atom cross-sectional area (cm^2), P_T is the total pressure (atm), N_A is Avogadro's number, M is the molecular weight of the adsorbate (g/mol), and R is the universal gas constant ((atm cm^3)/(mol K)). The sticking coefficient S_0 was calculated based on the data for CO adsorption on Pd(100) surface reported by Yeo et al. [30], who have shown that S_0 changes almost linearly with CO surface coverage (θ_{CO}), i.e.,

$$S_0 = 0.84 - 0.5375\theta_{CO}. \tag{20}$$

Because step 3 of the Langmuir–Hinshelwood reaction scheme is considered to be in equilibrium, the rate constant k_d can be calculated based on the thermodynamic constant K for CO chemisorption given by

$$K = \frac{k_d}{k_a} \Rightarrow k_a = \frac{k_d}{K}. \tag{21}$$

The thermodynamic constant K for CO chemisorption can be calculated using the following formula:

$$K = \exp(\Delta S^0/R)\exp(-\Delta H^0/RT), \tag{22}$$

where ΔS^0 is the entropy of CO chemisorption on Pd (J/(mol K)), and ΔH^0 is the enthalpy of CO chemisorption on Pd (J/mol). According to Shustorovich [31], in the 500–700 °C range, the entropy of CO chemisorption on Pd can be considered practically constant (∼ 30 cal/(mol K)). However, the enthalpy of CO chemisorption is reported to vary significantly with CO coverage [30] and can be approximated by

$$-\Delta H^0 = 172.7 - 13.0\theta_{CO} \quad (\text{kJ/mol}). \tag{23}$$

Table 6
Simulation results based on the Langmuir–Hinshelwood mechanism for the CO oxidation reaction (steps 3 and 4)

k_4	k_2^{app}	Ω	$\Re$	$N^0_{O-S_2}$ (μatom/g)	$N^0_{O-S_2}$ exp (μatom/g)	Comments
			$T = 500$ °C			
100,000	500	0.8977	0.9948	61.5	67.3	Highest value of Ω; θ_O and θ_{CO} drop to zero for $t > 0.2$ s
10	0.03	0.1321	0.9153	12.3	67.3	Reasonable variation of θ_O and θ_{CO} with time; not satisfactory value of Ω
			$T = 600$ °C			
70,000	320	0.8234	0.9914	58.2	158.0	Highest value of Ω; θ_O and θ_{CO} drop to zero for $t > 0.2$ s
5	0.01	0.0925	0.8756	11.1	158.0	Reasonable variation of θ_O and θ_{CO} with time; not satisfactory value of Ω

The main features of the simulation results after using the LH kinetics for CO oxidation are reported in Table 6. To obtain high values of parameter Ω, larger values for both k_4 and k_2^{app} were used than those of k_1 and k_2^{app} used with the ER kinetics. However, these values of k_4 and k_2^{app} resulted in practically zero surface coverages for both CO and oxygen at reaction times higher than 0.2 s. The result of zero oxygen coverage is inconsistent with the experimental results, which show that CO_2 production stops only at reaction times higher than about 10 s. To obtain more reasonable evolutions of θ_{CO} and θ_O, one must use significantly smaller values of both k_4 and k_2^{app}. However, in this case the value of Ω becomes significantly smaller ($\Omega < 0.15$), which is undesired. The estimated value of $N^0_{O-S_2}$ at 500 °C was 12.3 μatom/g, while the experimental value was 67.3 μatom/g. As shown in Table 6, similar results and conclusions were obtained for the reaction temperature of 600 °C. It is noted that changes in the estimated values of k_a and k_d via Eqs. (20)–(23) by an order of magnitude did not affect the conclusions reached for the LH kinetics presented in Table 6.

In conclusion, the simulation results obtained after assuming LH kinetics for the present transient CO oxidation reaction fail to reproduce the experimental pulse transient results of Fig. 4. The results shown in Figs. 4 and 9 and Table 6 strongly support the ER kinetic scheme presented by steps 1 and 2. Reaction step 1 is considered as a pure elementary reaction step, in the sense that it can occur on a molecular level [32].

Many theoretical studies have shown that the most energetically favorable (lowest reaction energy barrier) reaction path for the CO/O_2 reaction (co-fed CO and O_2 from the gas phase) over unsupported Pt, Pd, and Rh metal surfaces is that associated with the LH mechanism [33–39]. The reaction barrier was found to be in the range 50–140 kJ/mol, while the highest energy sub-barrier was identified as that of the weakening of the metal–oxygen bond [33–39]. In the case of supported Pt, Pd, and Rh catalysts, a LH kinetic model is usually found to best fit the experimental rate results for the CO/O_2 reaction at $T < 300\,^{\circ}C$ and for ratios of P_{CO}/P_{O_2} that correspond to not strongly oxidizing feed conditions [40–42].

The main differences in the conditions of the present transient CO oxidation reaction, which lead to ER kinetics, compared to those encountered under steady-state reaction conditions (CO/O_2 feed streams), which lead to LH kinetics for group VIII-supported metal catalysts [40–42], are the following:

1. In the present pulse transient experiments, there is no co-fed oxygen in the CO pulse.
2. Before CO is admitted to the reactor, the supported catalytic surface does not correspond to the state of metallic palladium but to that of PdO. This is based on results from the literature [20–23], where it has been demonstrated that at temperatures in the 350–800 °C range, exposure of Pd to an oxygen atmosphere (even at 0.2 Torr) leads to its conversion to PdO (surface and subsurface in many layers). Decomposition of PdO occurs only at $T > 800\,^{\circ}C$ [21,23].
3. CO chemisorption is not expected to take place on Pd sites of the PdO surface in the 500–700 °C range. It is noted that, even on a Pd surface, the coverage of CO chemisorption in the 500–700 °C range was found to be nonmeasurable based on in situ FTIR studies performed on the present Pd/CeO_2 catalyst. This result implies a very small or zero residence time for the adsorbed CO molecule.
4. Upon reaction of CO with a surface oxygen atom of PdO during the pulse experiment, a surface oxygen vacant site in the PdO is to be formed. It might be argued that this vacant site could be used for CO chemisorption. Thus, a LH mechanism could also be operable along with the ER mechanism for the reaction system. However, the facts that the PdO phase is supported on ceria, a material largely promoting the back-spillover of oxygen process, and that the chemisorption energy of CO on the oxygen vacancy is expected to be significantly lower than that of oxygen on Pd [38], indicate that the possibility of having a chemisorbed CO state on the present PdO/CeO_2 system must be rather small. This conclusion is consistent with the present simulation results with the LH kinetics that fail to reproduce the experimental CO pulse transient response (see Section 4.6, Table 6).

Bondzie et al. [43] have studied the kinetics of reduction of PdO (formed on a Pd(110) crystal face) by CO at low pressures (5×10^{-8} mbar) in the 340–420 K range. The Eley–Rideal step was considered in their kinetic analysis. A rate constant (k) was estimated for this step and the value of 14.1 ML/s was reported at 400 K. The unit of ML used in their analysis corresponded to 9.4×10^{14} atoms/cm^2. It is very instructive to compare this reported value of k at 400 K with that predicted from the results of the present work. Considering the present case of CO oxidation (or PdO reduction by CO) at 773 K, for the maximum value of the rate of CO oxidation (55.7 μatom/(g s), Fig. 6a), and the corresponding N_{O-S_1} (36.8 μatom/g) and y (0.006) values, a rate constant $k_1 = 5.42 \times 10^{-7}$ (g atom)/(cm^2 s) is calculated. In these calculations, a value of 2.3 m^2 Pd/g (based on dispersion and the site density for the Pd(111) crystal face), and the rate Eq. (15) were used. In the latter equation, the surface coverage θ is used instead of N_{O-S_1} to express the unit of rate constant k_1 in (g atom)/(cm^2 s) as that reported [43]. Based on the activation energy value of 9.2 kJ/mol calculated from the present work (Fig. 9), and assuming a pre-exponential factor for the k_1 rate constant independent of temperature, a value of $k_1 = 14.2 \times 10^{-8}$ (g atom)/(cm^2 s) is obtained at 400 K. This value is about 6.5 times larger than the value reported by Bondzie et al. [43]. This difference in the k value corresponds to a 6.2 kJ/mol difference in the activation energy for the Eley–Rideal step of the CO oxidation on PdO in the two studies.

Based on what is mentioned in the previous paragraph, the relatively low value of 9.2 kJ/mol for the activation energy of the elementary step, $CO(g) + O\text{–}S\ (PdO) \rightarrow CO_2(g)$, estimated in the high-temperature range of 773–973 K over the present PdO/CeO_2 system, is consistent with the value of 15.4 kJ/mol estimated over the unsupported PdO in the low-temperature range of 340–420 K. An interesting and important view for explaining the relatively low activation barrier of 9.2 kJ/mol obtained in the present work comes from the recent work of Hirsimäki et al. [44]. The authors have studied the energy-dependent transient reaction kinetics of CO oxidation over a preoxidized Pd(110) surface, where they propose that at high translational energies for the CO impinging molecules the energy and momentum transfer results in the weakening of the Pd–O bond, thereby leading into the lowering of the activation energy barrier and increased reaction rate. This view could partly explain the 6.2 kJ/mol difference in activation energy estimated for the elementary reaction step under consideration at 400 and 773 K.

In a recent detailed work on Pd(111) using XPS, STM, and TPD techniques, Zheng and Altman [45] have indicated multiple Pd–O surface and subsurface species with different activities toward CO oxidation. The existence of multiple Pd–O species has been postulated as an explanation for the complex behavior observed in Pd-catalyzed oscillatory behaviour of the CO oxidation reaction [46,47]. In the present kinetic model, only a single oxygen species ($O\text{–}S_1$) has been

considered in the Eley–Rideal step of the CO oxidation reaction to form CO_2. If under the high temperatures used in the present work for the oxidation of Pd to PdO more than one kind of Pd–O species was present at the start of the CO pulse experiment, then the activation energy value of 9.2 kJ/mol estimated may reflect an apparent value accounting for the reactivity of all Pd–O species. However, such a hypothesis cannot be proven since no data are available on the details of the surface/subsurface structure of PdO at temperatures in the 500–700 °C range.

In a recent work [48] concerning the development of a transient kinetic model for the CO oxidation reaction over a $Pt/Rh/CeO_2/\gamma\text{-}Al_2O_3$ three-way catalyst in the 120–160 °C range, the following elementary reaction steps, among others, were considered for fitting the transient CO and CO_2 experimental responses obtained following the switch 0.5 mol% O_2/He → 0.5 mol% CO/He:

$$CO(g) + O\text{–}S \leftrightarrow OCO\text{–}S, \quad \text{(step 5)}$$

$$OCO\text{–}S \rightarrow CO_2(g) + S. \quad \text{(step 6)}$$

Nibbelke et al. [48] reported the 12.1 kJ/mol and 20.5 s^{-1} values for the activation energy barrier and pre-exponential factor of the rate constant k associated with step 6, respectively. In addition, the activation energy and pre-exponential factor of the backward rate constant of reaction step 5 were reported to be 20.3 kJ/mol and 248 s^{-1}, respectively. The reaction steps 5 and 6 are closely related to the Eley–Rideal step 1, and the reported kinetic values are of the same order as those calculated in the present work over the Pd/CeO_2 catalyst.

The suggestions of Böttcher et al. [37] for explaining the high CO oxidation reaction rate on a pre-oxidized Ru(0001) surface with 5 ML of oxygen species could also be adopted in the present case of the Pd/CeO_2 catalyst. The authors suggested that the interaction between subsurface oxygen atoms and overlayer oxygen atoms is repulsive, and as a result of this, the on-surface O atoms are markedly destabilized. Consequently, the activation energy of the CO oxidation (Eley–Rideal step) drops with respect to that with one monolayer ((1×1)–O overlayer) of oxygen atoms, giving rise to a significantly enhanced CO_2 production rate [37].

Relatively low activation energy barriers for true reaction elementary steps have recently been reported by Dumesic et al. [49] for the SCR of NO by NH_3 on vanadium oxide catalysts. A value of 19 kJ/mol was reported (based on density functional theory (DFT) calculations) for the conversion of the NH_3NHO adsorbed intermediate species to the NH_2NO one. To our knowledge, there are no theoretical estimates in the literature for the energetics of an ER mechanism for the CO oxidation over a PdO surface, to which we could compare the value of 9.2 kJ/mol calculated in the present work. This could be a challenge for future DFT studies on the present catalytic system.

It is useful to cite here certain works on the CO oxidation reaction over transition metal surfaces where the ER mechanism was found to support the experimental observations, where the oxygen partial pressure was larger than that of CO or the initial metal surface state was that corresponding to a high initial oxygen coverage. Dwyer and Bennett [50] in their transient CO oxidation studies with FTIR have found that an ER process initially proceeded when CO(g) reacted with pre-adsorbed oxygen in the 100–160 °C range over 9 wt% Pt/SiO_2 catalyst, while as CO accumulated on the surface the controlling mechanism shifted to the LH one. Bonzel and Ku [51] have studied the CO oxidation reaction on the Pt(110) surface and found that the temperature dependence of the CO_2 reaction rate exhibits a maximum, the position of which depends on the composition of the gas phase. At 215 °C, two different rate laws have been established depending on the ratio of P_{O_2}/P_{CO}. These authors claim that their results support the idea that the reaction obeys an Eley–Rideal mechanism for the experimental conditions investigated [44]. Finally, Srivastava et al. [52] have studied the oxidation of CO on Ni clusters by means of CNDO MO calculations. The cluster surface was pre-adsorbed with O and the variation of various bond energies with the approach of a CO molecule was investigated for different models. Srivastava et al. [52] found that, at high oxygen coverage, an Eley–Rideal reaction pathway is more probable.

4.7. Parametric sensitivity analysis

The effects of the total molecular flow (F_T) and of the initial amounts of surface adsorbed oxygen on PdO ($N^0_{O-S_1}$) and on cerium oxide ($N^0_{O-S_2}$) on the fitting of the pulse transient response of gaseous CO (y_{CO}) and the derived rate constants k_1 and k_2^{app} in the case of the ER kinetics were investigated. The F_T, $N^0_{O-S_1}$, and $N^0_{O-S_2}$ parameters are considered to present some experimental error in their determination. Table 7 presents the results obtained after allowing a 10% variation in the value of the above-mentioned three parameters. It is clearly seen that the percentage of error in determining the k_1 and k_2^{app} parameters is less than 0.6% and 12%, respectively. These results are indeed very im-

Table 7
Effects of the parameters F_T, $N^0_{O-S_1}$, and $N^0_{O-S_2}$ on the kinetic rate constants k_1 and k_2^{app} of the Eley–Rideal mechanism

Parameter value			Ω	k_1	k_2^{app}
F_T (μmol/s)	$N^0_{O-S_1}$ (μatom/g)	$N^0_{O-S_2}$ (μatom/g)		(s^{-1})	(s^{-1})
68.2	57.7	68.3	0.9948	304.0	3.2
61.4[a]	57.7	68.3	0.9935	304.0	3.0
75.0[b]	57.7	68.3	0.9942	304.0	3.3
68.2	51.9[a]	74.0	0.9949	304.0	3.4
68.2	63.5[b]	62.5	0.9946	302.0	2.9
68.2	57.7	61.4[a]	0.9944	304.0	3.1
68.2	57.7	75.1[b]	0.9945	304.0	3.3

[a] 10% decrease in the actual experimental value.
[b] 10% increase on the actual experimental value.

portant in establishing the reliability of the present kinetic model. The estimated transient rates of CO oxidation and back-spillover of the oxygen process and the corresponding calculated intrinsic rate constants k_1 and k_2^{app} are proven to be rather insensitive to the extent of possible experimental errors related to the performance of the CO pulse transient experiments in measuring the OSC phenomenon.

5. Conclusions

The following conclusions can be derived from the present work.

1. A mathematical model of the oxygen storage capacity (OSC) phenomenon on a model 1 wt% Pd/CeO_2 catalyst in a CO pulse injection experiment has been developed for the first time.
2. The proposed mathematical model allows the calculation of the transient rates (μmol/(s g)) of CO oxidation and back-spillover of the oxygen process during the pulse experiments. This important information cannot be extracted directly from the experiment. A comparison of the two reaction rates shows that as the reaction temperature increases from 500 to 700 °C, the rate value of the back-spillover of the oxygen process approaches that of the CO oxidation reaction.
3. It was found that the Eley–Rideal mechanism for the CO oxidation in the 500–700 °C range over supported PdO on ceria describes very well the experimental pulse transient response of CO. This mechanism is also supported by in situ FTIR experiments. The intrinsic activation energy for the Eley–Rideal step of CO oxidation is found to be 9.2 kJ/mol.
4. Despite the fact that the ratio of the rate of CO oxidation to that of the back-spillover of oxygen is in the range 1.2–3.0, the ratio of the corresponding rate constants is about 100. This is an important result, indicating that one cannot use the values of the rate constants of the two processes to compare the corresponding transient rates. This is simply due to the fact that the initial oxygen reservoir on ceria is significantly larger than the initial oxygen reservoir on PdO. In addition, the transient rates at hand are determined by different kinetics, the dynamics of which appear to be significantly different (see Fig. 5 and Eqs. (1)–(6)).
5. The results of the present work can be used to gain a better understanding of the effects of various additives and contaminants on PM (Pt, Pd, Rh) supported on ceria catalysts, or related catalytic systems that promote the oxygen storage capacity phenomenon, on the transient rates of CO or hydrocarbon oxidation and back-spillover of the oxygen process.

Acknowledgments

Financial support by the European Union (Contract No. G5RD-CT-2000-00376) and the Research Committee of the University of Cyprus is gratefully acknowledged. The research group of Prof. C.R. Theocharis (University of Cyprus) for carrying out the BET measurements and the useful discussions with Prof. M. Mavrikakis (University of Wisconsin-Madison, USA) are also acknowledged.

References

[1] K.C. Taylor, in: J.R. Anderson, M. Boudart (Eds.), Catalysis Science and Technology, Vol. 5, Springer, Berlin, 1986, Chapt. 2.
[2] B. Harrison, A.F. Diwell, C. Hallett, Platinum Met. Rev. 32 (1988) 73.
[3] G. Vlaic, R. Di Monte, P. Fornasiero, E. Fonda, J. Kaspar, M. Graziani, Stud. Surf. Sci. Catal. 116 (1998) 185.
[4] D. Duprez, C. Descorme, T. Birchem, E. Rohart, Top. Catal. 16/17 (2001) 49.
[5] H.C. Yao, Y.F. Yu Yao, J. Catal. 86 (1984) 254.
[6] B. Engler, E. Koberstein, P. Schubert, Appl. Catal. 48 (1989) 71.
[7] G. Vlaic, P. Fornasiero, S. Geremia, J. Kaspar, M. Graziani, J. Catal. 168 (1997) 386.
[8] J. Kaspar, R. Di Monte, P. Fornasiero, M. Graziani, H. Bradshaw, C. Norman, Top. Catal. 16/17 (2001) 83.
[9] G. Balducci, P. Fornasiero, R. Di Monte, J. Kaspar, S. Meriani, M. Graziani, Catal. Lett. 33 (1995) 193.
[10] T. Miki, T. Ogawa, M. Haneda, N. Kakuta, A. Ueno, J. Phys. Chem. 94 (1990) 6464.
[11] N. Kakuta, N. Morishima, M. Kotobuki, T. Iwase, T. Mizushima, Y. Sato, S. Matsuura, Appl. Surf. Sci. 121/122 (1997) 408.
[12] E.C. Su, C.N. Montreuil, W.G. Rothschild, Appl. Catal. 17 (1985) 75.
[13] S. Kacimi, J. Barbier Jr., R. Taha, D. Duprez, Catal. Lett. 22 (1993) 343.
[14] S. Bedrane, C. Descorme, D. Duprez, Catal. Today 75 (2002) 401.
[15] C.N. Costa, T. Anastasiadou, A.M. Efstathiou, J. Catal. 194 (2000) 250.
[16] D.M. Stockwell, J.S. Chung, C.O. Bennett, J. Catal. 112 (1988) 135.
[17] A.M. Efstathiou, PhD thesis, University of Connecticut, USA, 1989.
[18] J.M. Gatica, R.T. Baker, P. Fornasiero, S. Bernal, J. Kašpar, J. Phys. Chem. B 105 (2001) 1191.
[19] J.J.F. Scholten, A.P. Pijpers, A.M.L. Hustings, Catal. Rev.-Sci. Eng. 27 (1) (1985) 151.
[20] N.M. Rodriguez, S.G. Oh, R.A. Dalla-Betta, R.T.K. Baker, J. Catal. 157 (1995) 676.
[21] J.J. Chen, E. Ruckenstein, J. Phys. Chem. 85 (1981) 1606.
[22] H. Lieske, J. Volter, J. Phys. Chem. 89 (1985) 1841.
[23] M. Chen, L.D. Schmidt, J. Catal. 56 (1979) 198.
[24] C. Li, K. Domen, K. Maruya, T. Onishi, J. Catal. 123 (1990) 436.
[25] M. Che, A.J. Tench, in: D.D. Eley, H. Pines, P.B. Weisz (Eds.), Advances in Catalysis, Vol. 32, Academic Press, San Diego, CA, 1983.
[26] M. Bowker, L.J. Bowker, R.A. Bennett, P. Stone, A. Ramirez-Cuesta, J. Mol. Catal. 163 (2000) 221.
[27] J.M. Smith, Chemical Engineering Kinetics, McGraw–Hill, New York, 1970.
[28] C.G. Vayenas, G.E. Pitselis, Ind. Eng. Chem. Res. 40 (2001) 4209.
[29] A.M. Efstathiou, C.O. Bennett, J. Catal. 124 (1990) 116.
[30] Y.Y. Yeo, L. Vattuone, D.D. King, J. Chem. Phys. 106 (5) (1996) 1.
[31] E. Shustorovich, Metal-Surface Reaction Energetics, VCH, New York, 1991.
[32] M. Boudart, G. Djega-Mariadassou, Kinetics of Heterogeneous Catalytic Reactions, Princeton University Press, Princeton, NJ, 1981.
[33] A. Eichler, Surf. Sci. 498 (2002) 314.
[34] A. Eichler, J. Hafner, Phys. Rev. B 59 (8) (1999) 5960.
[35] A. Alavi, P. Hu, T. Deutsch, P.L. Silvestrelli, J. Hutter, Phys. Rev. Lett. 80 (16) (1998) 3650.
[36] P. Salo, K. Honkala, M. Alatalo, K. Laasonen, Surf. Sci. 516 (2002) 247.
[37] A. Böttcher, H. Niehus, S. Schwegmann, H. Over, G. Ertl, J. Phys. Chem. B 101 (1997) 11185.

[38] C. Stampfl, M. Scheffler, Phys. Rev. Lett. 78 (8) (1997) 1500.
[39] C.H.F. Peden, D.W. Goodman, M.D. Weisel, F.M. Hoffmann, Surf. Sci. 253 (1991) 44.
[40] S.B. Schwartz, L.D. Schmidt, G.B. Fisher, J. Phys. Chem. 90 (1986) 6194, and references therein.
[41] T. Ioannides, A.M. Efstathiou, Z.L. Zhang, X.E. Verykios, J. Catal. 156 (1995) 265.
[42] M.B. Cutlip, C.J. Hawkins, D. Mukesh, W. Morton, C.N. Kenney, Chem. Eng. Commun. 22 (1983) 329, and references therein.
[43] V.A. Bondzie, P.H. Kleban, D.J. Dwyer, Surf. Sci. 465 (2000) 266.
[44] M. Hirsimäki, P. Nieminen, M. Valden, Surf. Sci. 482–485 (2001) 147.
[45] G. Zheng, E.I. Altman, Surf. Sci. 462 (2000) 151.
[46] M.R. Bassett, R. Imbihl, J. Chem. Phys. 93 (1990) 811.
[47] E.I. Latkin, V.I. Elokhin, A.V. Matveev, V.V. Gorodetskii, J. Mol. Catal. A 158 (2000) 161.
[48] R.H. Nibbelke, A.J.L. Nievergeld, J.H.B.J. Hoebink, G.B. Marin, Appl. Catal. B: Environ. 19 (1998) 245, and references therein.
[49] M. Anstrom, N.Y. Topsøe, J.A. Dumesic, J. Catal. 213 (2003) 115.
[50] S.M. Dwyer, C.O. Bennett, J. Catal. 75 (1982) 275.
[51] H.P. Bonzel, R. Ku, J. Vac. Sci. Technol. 9 (1972) 663.
[52] A.K. Srivastava, I. Kojima, E. Miyazaki, Bull. Chem. Soc. Jpn. 59 (11) (1986) 3375.